Comparative Study of the Effect of the Compression and Traction Loads on the Stress and Deformation of a Toroidal LPG Tank

Assistant professor PhD. Eng. **Petre OPRIŢOIU**

Technical University of Cluj-Napoca, Department of MTC, Observatorului Street, no. 72-74, Cluj-Napoca, 400363, Cluj county, Romania. Corresponding author* e-mail: petre.opritoiu@mtc.utcluj.ro

Abstract: *The aim of this research is to identify similarities and differences between the stress and deformation behaviors of a three-dimensional (3-D) hexagonal toroid with a regular hexagonal cross-section used in the manufacturing of liquefied petroleum gas (LPG) storage tanks from the automotive industry under compression and traction loads using the finite element simulations. Compression and traction loads applied to the structural design of a storage tank are according to its intended use, size, structure type, materials, design lifetime, in order to assure product safety and to maintain its essential functions. Numerical simulations of the influence of compression, traction loads, and temperature for a given situation considering the 3-D geometry model are used to explain observed phenomena, explore the limitations of various approaches, improved techniques, and technology, and assure the safety of LPG storage tanks. Higher temperature changes and the thermal gradient between the surface layer and the inner layer of material can determine the modification of the mechanical properties of the material and can lead to the formation of fine cracks. The storage tank design model is formulated, according geometrical, mechanical and thermal aspects, to minimize the storage tank mass in terms of thermal performance and safety aspects. The quantitative computational approaches based on the design specifications and standards were used to evaluate the product performance as well as the accuracy of results. The approach proposed by the authors enables a significant reduction in the computational time and makes it possible to perform complex numerical simulations for various 3-D models. The research results besides numerical comparisons, provide a clear basis for interpreting and understanding the relevance of this research method in design of LPG storage tanks.*

Keywords: *3-D hexagonal toroidal LPG fuel tank, compression and traction loads, automotive industry, industrial engineering design, optimization methods, finite element analysis*

1. Introduction

Computer-aided manufacturing (CAM) and computer-aided design (CAD) play a central role in developing the fuel storage tanks market from the automotive industry, to provide high-quality products and to fully satisfy customer needs and expectations [1-3].

In computer-aided design (CAD) of production models [4-7], innovative approaches are needed to satisfy the global market growth, while simultaneously reducing production costs, in correlation with quality requirements and security legislation [8-11].

Three-dimensional (3-D) CAD models not only provide geometry information for different geometrical variants of liquefied petroleum gas (LPG) storage tanks [12-15], but also serve as the basis for module configuration [16-19], as well as for various simulation [20-22], verification processes [23-25] and quality control [24-26].

Finite element analysis (FEA) is a computational tool [27-29] in engineering to design [30-32] and failure analysis to calculate the strength and behavioral characteristics of a material under various conditions, and to investigate large-scale and small-scale behaviors of materials.

This modern tool provides many useful advantages for numerical stress analysis, with an advantage of being applicable to solids of irregular geometry that contain heterogeneous material properties, not for replacements for experimental techniques. Also, the 3-D computational model [33, 34] can be tested under different conditions, under various simple or combined static or dynamic loads, and the simulation results can allow a fast, accurate comparison of numerous results for integrated product development.

In general, computational studies in fluid mechanics [35-38] and heat transfer processes of LPG storage tanks have a major benefit in geometrical optimization [39-42], fluid-structure interaction modelling, and improved product quality.

According to the scientific literature of (LPG) storage tanks, rare studies were devoted to the compression and traction loads of 3-D hexagonal toroid with a regular hexagonal cross-section, or combined deformation behaviors using the finite element simulations.

The objectives of this study are as follows: (1) to develop a simplified 3-D model for the compression and traction loads, (2) to study computationally the role of the main geometric parameters and temperature to give preliminary recommendation on optimization of engineering solutions for manufacturing, (3) to present a numerical solution for realistic case study.

2. Design methodology

2.1. Basic geometry of the parametric 3-D model

Let's consider the parametric 3-D model generated by revolving of a closed generating curve C_G (a hexagon with rounded corners) along a closed guiding curve C_D (a hexagon with rounded corners) as shown in fig. 1 [14].

The following parameters were applied as input parameters to the 3-D parametric model (figs. 1 and 2): a) a closed generating curve CG (a hexagon with a side value L = 175 mm, with rounded corners, radius R = 50 mm), and b) the guiding curve CD (a hexagon with a side value L = 430 mm, with rounded corners, radius R = 180 mm), and the thickness = 10 mm.

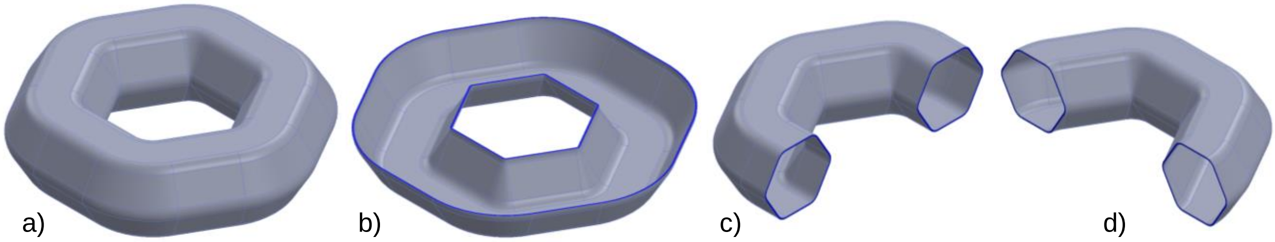

Fig. 1. The isometric representation of non-deformed 3-D model: a) view; b), c) and d) different sections

Based on the physical model, the modeling was done in the AutoCAD Autodesk 2020 software and the numerical analysis was performed with SolidWorks 2020 software with the Static, Thermal and Design Study modules. The design data used were:

- the tank material is AISI 4340 steel;
- the maximum hydraulic test pressure: p_{max} = 30 bar;
- the working temperature between the limits: T = -30 ^{0}C up to T = 60 ^{0}C;
- supporting surfaces located on the inferior side;
- the duration of the tank exploitation: n_a = 15 years;
- the corrosion rate of the material: v_c = 0.07 mm/year.

The numerical analyses of the influence of uniaxial compression and traction loads were studied in references [20, 22], considering for ΔL = 1.33% from the average diameter of the 3-D model, measured in the direction of deformation (figs. 2 and 3).

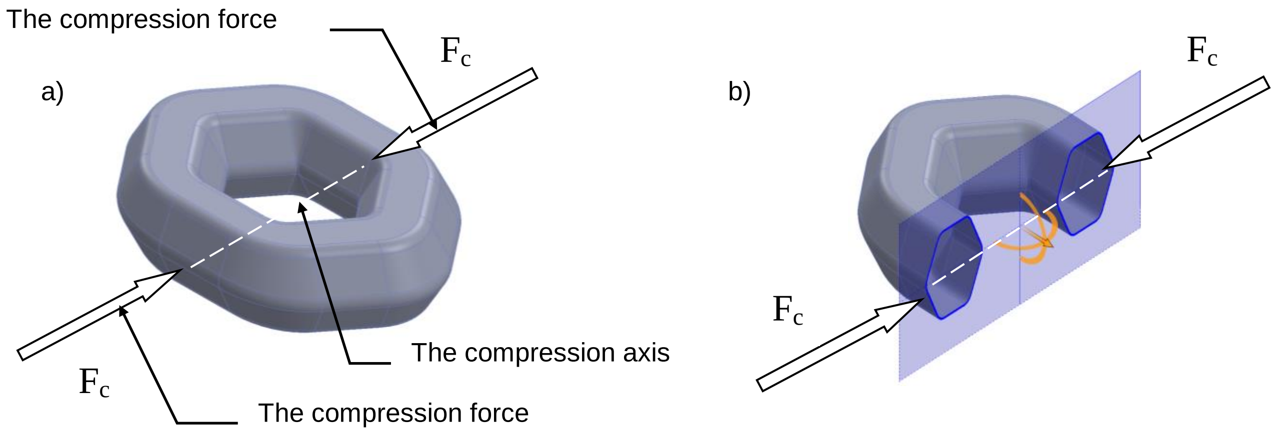

Fig. 2. The isometric representation of deformed 3-D model, after the uniaxial compression: a) view; b) cross section

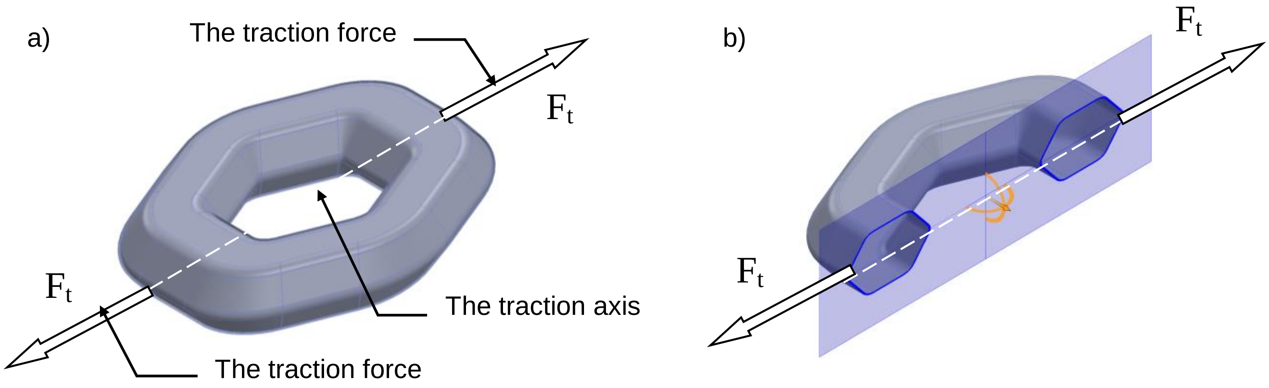

Fig. 3. The isometric representation of deformed 3-D model, after the uniaxial traction: a) view; b) cross section

The uniaxial displacement under compression or traction loads is noted with L_c.

As can be seen in the qualitative deformation of the 3-D model, for the case of compression loads the height of the cross section increases; while for the traction loads, the height of the cross section decreases. Both types of deformations determine directly, additional Von Mises resultant efforts and additonal resulting linear deformations of the 3-D model, greater than the maximum admissible limits of material.
It can be seen that the compression and traction loads are applied normally on the parallel sides of the model by means of the tangent planes (fig. 4 and 5), in addition to the affecting factors (temperature and corrosion process).

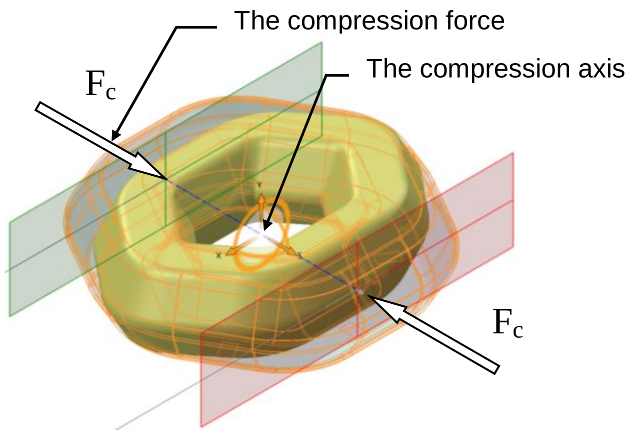

Fig. 4. The isometric representation of 3-D model, deformed, after the uniaxial compression

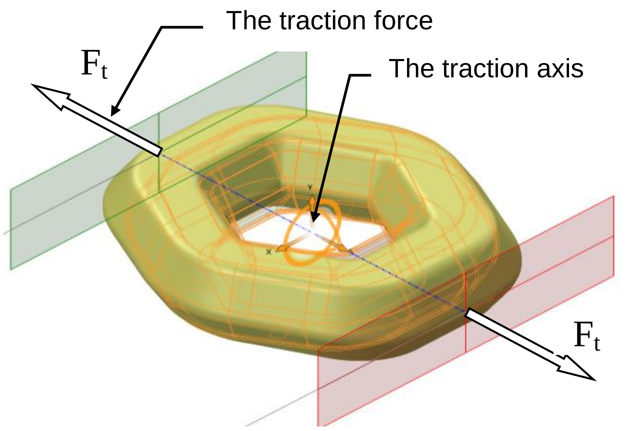

Fig. 5. The isometric representation of 3-D model, deformed, after the uniaxial traction

Numerical calculations were performed for: mesh standard type, solid mesh, curvature-based mesh with quality high, Jacobian in 16 points, element size 11 mm, number of nodes 30628, number of elements 15368. The Von Mises resultant efforts were calculated in both cases of deformations (compression and traction loads) in references [20, 22] and shown in table 1.

Table 1: The Von Mises resultant effort for: T = {-30 ^{0}C, 0 ^{0}C, 30 ^{0}C, 60 ^{0}C} and n_a= {0, 5, 10 and 15 years}

n_a [years]	$L_{c,t}$ [mm]	T [°C]				T [°C]			
		-30°	0°	30°	60°	-30°	0°	30°	60°
		σ_c [MPa] / the compression loads				σ_t [MPa] / the traction loads			
0	0	665.40	565.66	479.29	527.43	665.40	565.66	479.29	527.43
	1	639.82	542.94	515.96	557.23	545.22	470.35	485.68	541.97
	2	627.93	527.30	500.92	546.85	505.58	443.67	466.81	527.46

	3	531.38	467.79	507.29	549.93	521.01	448.29	487.10	540.16
	4	509.47	464.14	508.40	556.37	531.82	457.71	473.33	527.49
	5	589.15	499.13	448.13	452.74	529.59	455.52	488.13	546.48
	6	674.86	570.83	512.66	561.59	524.46	492.94	474.49	531.09
	7	651.59	550.74	504.76	547.34	657.82	559.64	485.78	538.97
	8	525.77	472.30	516.00	563.23	619.07	524.38	468.05	468.05
	9	523.78	529.17	521.79	570.21	523.90	446.61	466.19	521.03
	10	568.13	533.82	498.05	543.62	522.72	444.74	470.08	527.07
5	0	610.22	514.24	511.09	560.58	610.22	514.24	511.09	560.58
	1	532.28	510.09	552.49	598.10	593.51	502.09	506.01	563.14
	2	564.98	521.91	562.62	606.45	534.81	472.72	510.20	556.49
	3	631.33	538.41	557.01	600.40	584.30	502.98	514.43	571.78
	4	678.74	578.54	544.43	591.21	546.24	474.59	525.31	588.70
	5	665.32	564.82	559.06	604.03	565.15	486.81	500.36	558.24
	6	674.56	570.71	512.09	542.58	602.07	524.28	521.33	578.30
	7	679.16	578.01	478.09	488.02	576.45	494.93	478.15	522.33
	8	674.37	570.86	494.20	528.26	704.33	604.23	505.07	559.88
	9	646.48	550.40	559.13	600.81	691.79	591.13	502.17	556.59
	10	649.97	555.16	560.20	596.27	589.18	514.04	507.66	568.22
10	0	656.26	615.97	591.97	641.72	656.26	615.97	591.97	641.72
	1	566.98	568.67	606.88	647.44	718.61	623.72	586.50	632.99
	2	577.49	580.21	623.99	670.84	585.76	509.56	535.62	587.22
	3	680.81	585.12	611.01	658.16	591.81	516.25	567.98	623.54
	4	690.24	589.25	601.49	655.87	722.39	623.49	525.83	545.66
	5	703.44	600.73	635.70	675.09	602.64	531.32	576.29	642.99
	6	698.80	601.83	608.11	652.30	737.04	738.28	740.10	742.49
	7	677.61	593.07	639.09	690.45	587.54	510.56	528.33	559.51
	8	657.19	565.88	533.39	570.39	683.04	585.06	555.56	609.76
	9	589.70	547.00	578.70	613.37	584.59	509.34	584.59	585.40
	10	581.48	563.95	606.61	652.00	581.63	505.67	511.08	561.02
15	0	754.50	655.70	636.94	688.12	754.50	655.70	636.94	688.12
	1	760.74	661.69	677.69	720.92	680.88	589.79	591.14	638.86
	2	733.97	630.11	636.39	671.18	760.61	669.24	628.56	679.21
	3	608.07	618.41	658.21	700.28	657.33	583.00	643.56	708.33
	4	618.59	636.51	681.17	728.32	640.55	566.19	600.51	644.61
	5	644.32	579.84	618.48	662.06	660.04	586.78	622.83	658.88
	6	633.14	632.84	599.81	627.73	602.60	572.32	634.55	700.08
	7	640.52	627.79	669.36	713.72	636.33	567.02	565.91	573.71
	8	667.74	655.60	703.00	754.60	695.16	592.73	556.54	591.79
	9	624.54	623.04	667.02	713.53	789.42	683.81	579.95	597.50
	10	599.76	618.13	661.29	707.00	735.27	637.78	542.83	590.54

2.2. Numerical analysis of the parametric 3-D model

The graphs of curves corresponding to the Von Mises resultant efforts $\sigma_{c,t}$ (L_c, T) are graphically shown in fig. 6, for n_a = {0, 5, 10, and 15 years} and T = {-30 ^{0}C, 0 ^{0}C, 30 ^{0}C, 60 ^{0}C}.

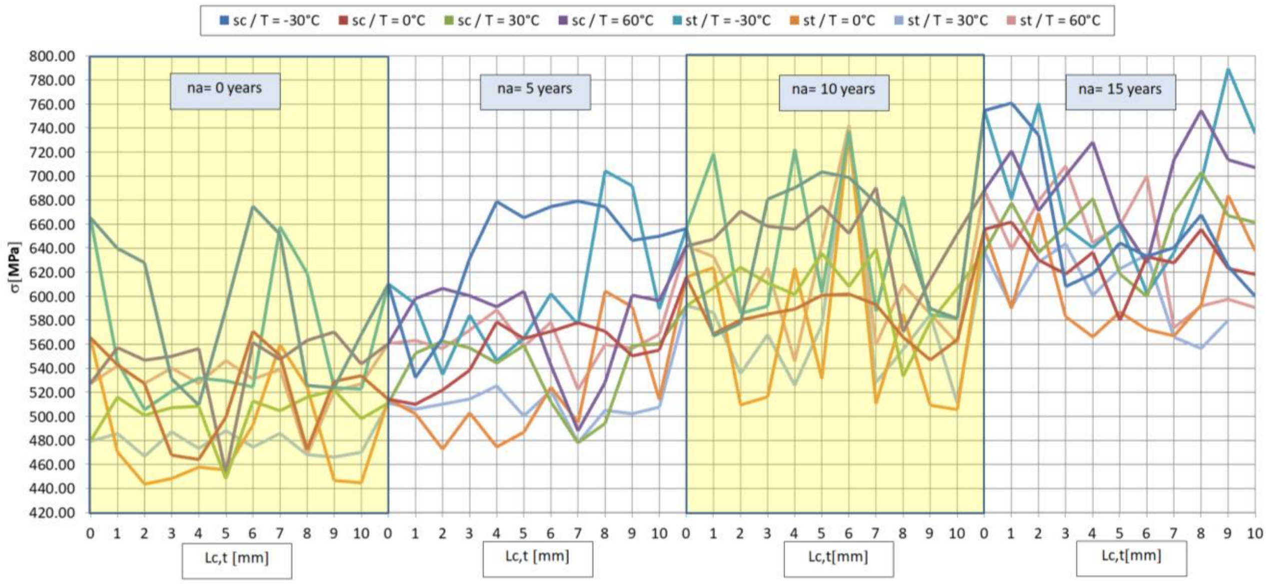

Fig. 6 The graphs of the Von Mises resultant efforts with highlighted details:
(T = 60 ^{0}C; n_a= {0, 5, 10 and 15 years}; T = {-30 ^{0}C, 0 ^{0}C, 30 ^{0}C, 60 ^{0}C}})

The 3-D graphs corresponding to the Von Mises resultant efforts $\sigma_{c,t}$ (L_c, T) taking into account the results from table 1 are graphically shown in figs. 7-10, respectively.

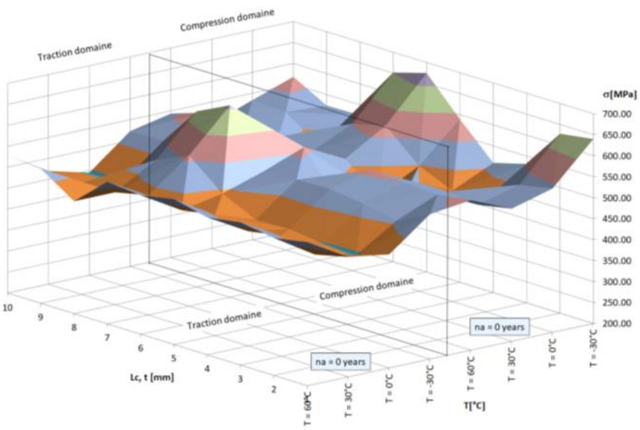

Fig. 7. The graphs of σ = f(L_c, T) for n_a = 0 years
left (traction domain); right (compression domain)

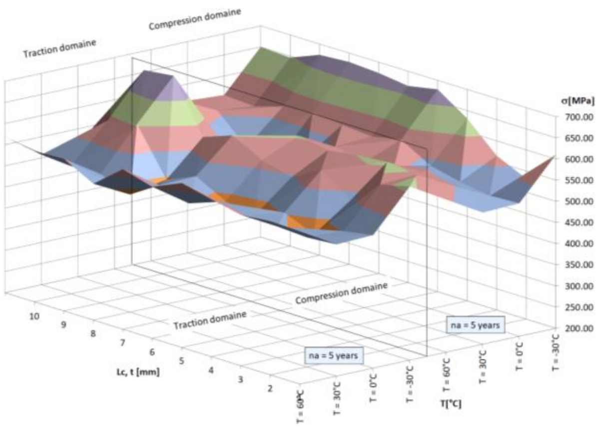

Fig. 8. The graphs of σ = f(L_c, T) for n_a = 5 years
left (traction area); right (compression area)

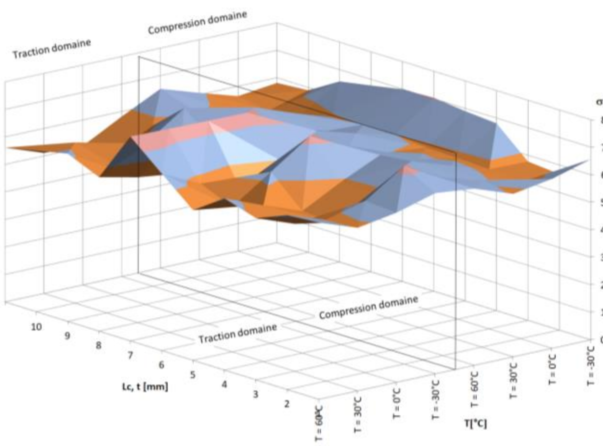

Fig. 9. The graphs of σ = f(L_c, T) for n_a = 10 years
left (traction domain); right (compression domain)

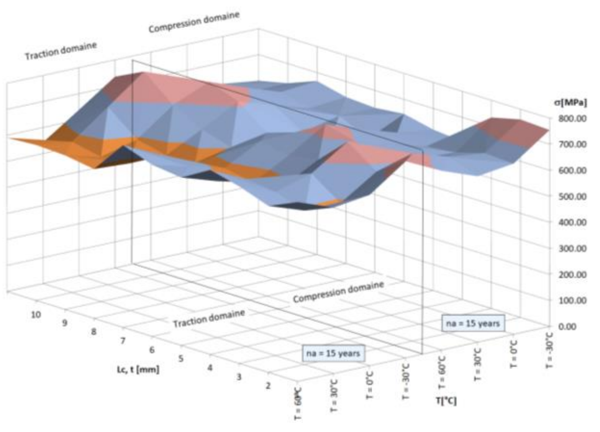

Fig. 10. The graphs of σ = f(L_c, T) for n_a = 15 years
left (traction area); right (compression area)

The graphs of curves $\sigma = f(L_c, T)$ with these highlighted details are shown in figs. 11-14.

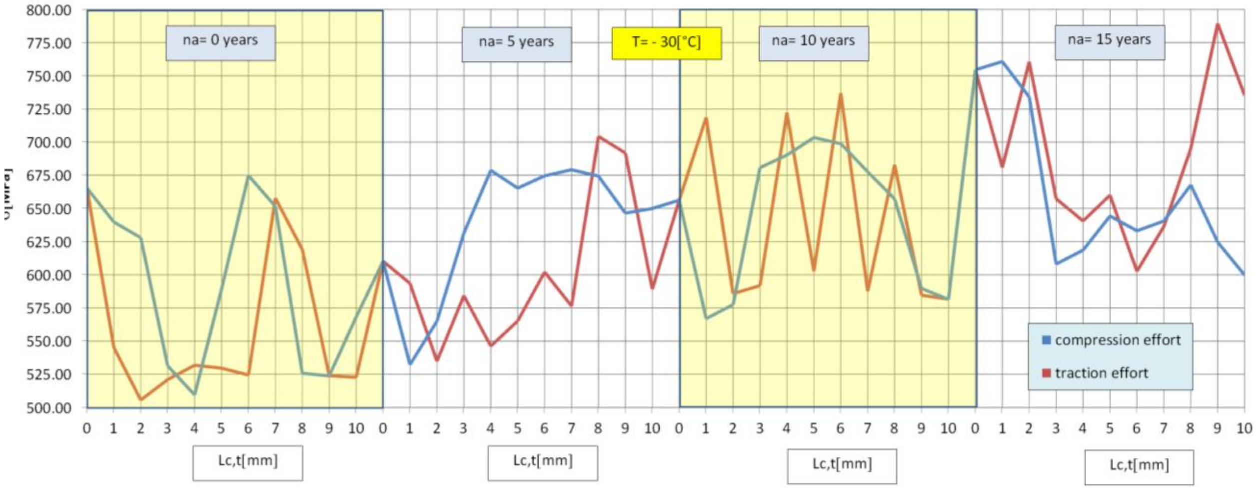

Fig. 11. The graphs of the Von Mises resultant efforts $\sigma = f(L_c, T)$ with highlighted details:
(T = -30 ^{0}C; n_a= {0, 5, 10 and 15 years}; blue curve – the compression effort; red curve – the traction effort;

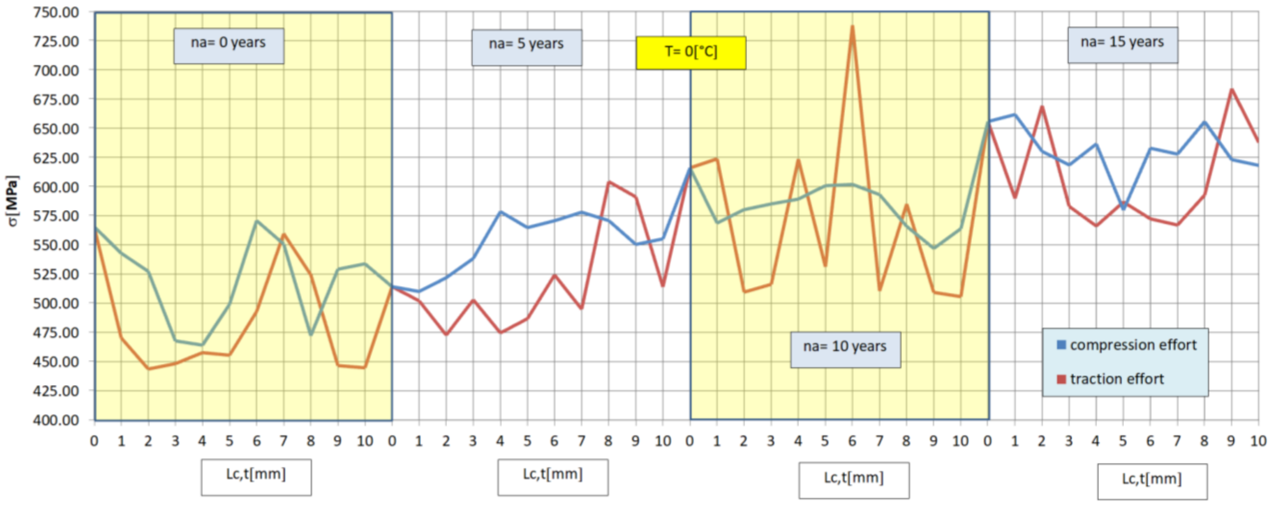

Fig. 12. The graphs of the Von Mises resultant efforts $\sigma = f(L_c, T)$ with highlighted details:
(T = 0 ^{0}C; n_a= {0, 5, 10 and 15 years}; blue curve – the compression effort; red curve – the traction effort;

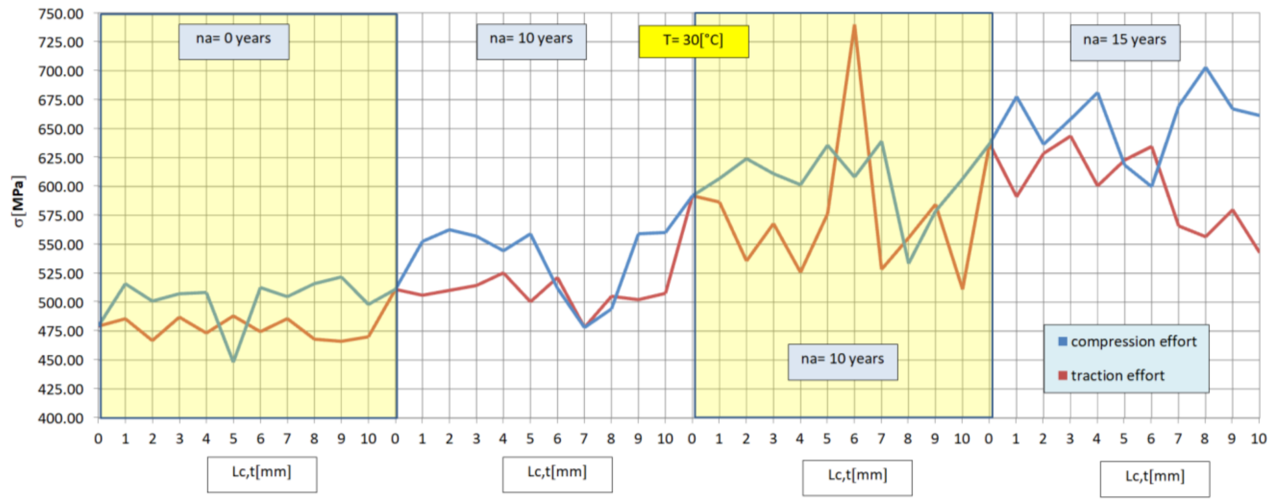

Fig. 13. The graphs of the Von Mises resultant efforts $\sigma = f(L_c, T)$ with highlighted details:
(T = 10 ^{0}C; n_a= {0, 5, 10 and 15 years}; blue curve – the compression effort; red curve – the traction effort;

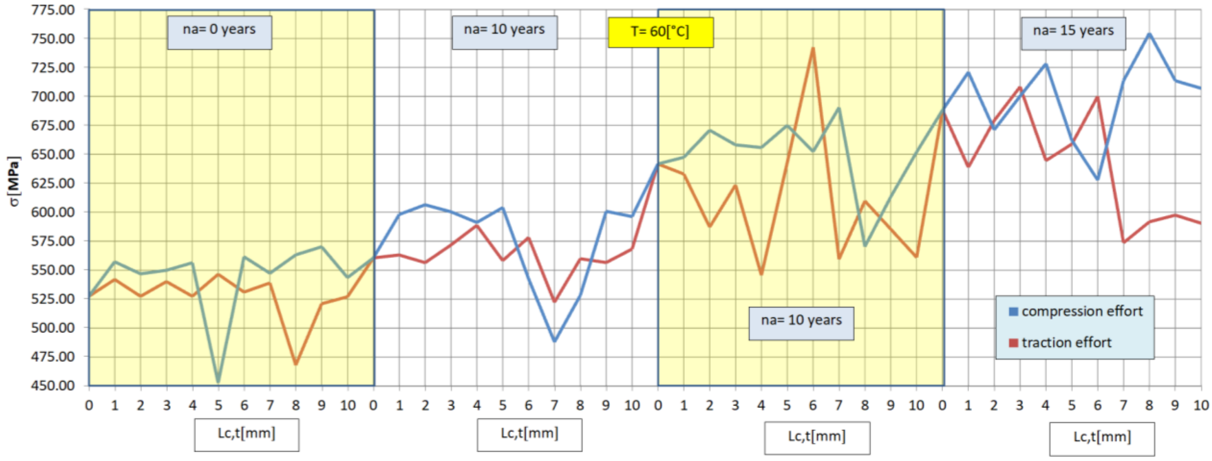

Fig. 14. The graphs of the Von Mises resultant efforts $\sigma = f(L_c, T)$ with highlighted details:
($T = 60\ ^0C$; $n_a = \{0, 5, 10$ and 15 years$\}$; blue curve – the compression effort; red curve – the traction effort.

It was calculated the percentage variation of the Von Mises effort $\Delta\sigma$ (L_c, T) given by compression versus the resulting stress state given by traction, using the following formula:

$$\Delta\sigma = \frac{(\sigma_c - \sigma_t)}{\sigma_t} \cdot 100\ [\%] \tag{1}$$

The percentage variation of Von Mises resultant effort $\Delta\sigma$ was computed in table 2 and the corresponding graphs (in 2-D) are shown in fig. 15.

Table 2: The percentage variation ($\Delta\sigma$) of the Von Mises effort for:
T = {-30 ^{0}C, 0 ^{0}C, 30 ^{0}C, 60 ^{0}C} and n_a= {0, 5, 10 and 15 years}

$L_{c,t}$ [mm]	T [°C]				T [°C]			
	-30°	0°	30°	60°	-30°	0°	30°	60°
	Δσ [MPa]				Δσ [MPa]			
	n_a = 0 [years]				n_a = 5 [years]			
1	17.35	15.43	6.23	2.82	-10.32	1.59	9.19	6.21
2	24.20	18.85	7.31	3.68	5.64	10.41	10.27	8.98
3	1.99	4.35	4.14	1.81	8.05	7.05	8.28	5.01
4	-4.20	1.40	7.41	5.48	24.26	21.90	3.64	0.43
5	11.25	9.57	-8.19	-17.15	17.72	16.03	11.73	8.20
6	28.68	15.80	8.05	5.74	12.04	8.86	-1.77	-6.18
7	-0.95	-1.59	3.91	1.55	17.82	16.79	-0.01	-6.57
8	-15.07	-9.93	10.24	20.33	-4.25	-5.52	-2.15	-5.65
9	-0.02	18.49	11.93	9.44	-6.55	-6.89	11.34	7.94
10	8.69	20.03	5.95	3.14	10.32	8.00	10.35	4.94
	n_a = 10 [years]				n_a = 15 [years]			
1	-21.10	-8.83	3.47	2.28	11.73	12.19	14.64	12.85
2	-1.41	13.86	16.50	14.24	-3.50	-5.85	1.24	-1.18
3	15.04	13.34	7.58	5.55	-7.49	6.07	2.28	-1.14
4	-4.45	-5.49	14.39	20.20	-3.43	12.42	13.43	12.99
5	16.73	13.06	10.31	4.99	-2.38	-1.18	-0.70	0.48
6	-5.19	-18.48	-17.83	-12.15	5.07	10.57	-5.48	-10.33
7	15.33	16.16	20.96	23.40	0.66	10.72	18.28	24.41
8	-3.79	-3.28	-3.99	-6.46	-3.94	10.61	26.32	27.51
9	0.87	7.40	-1.01	4.78	-20.89	-8.89	15.01	19.42
10	-0.03	11.53	18.69	16.22	-18.43	-3.08	21.82	19.72

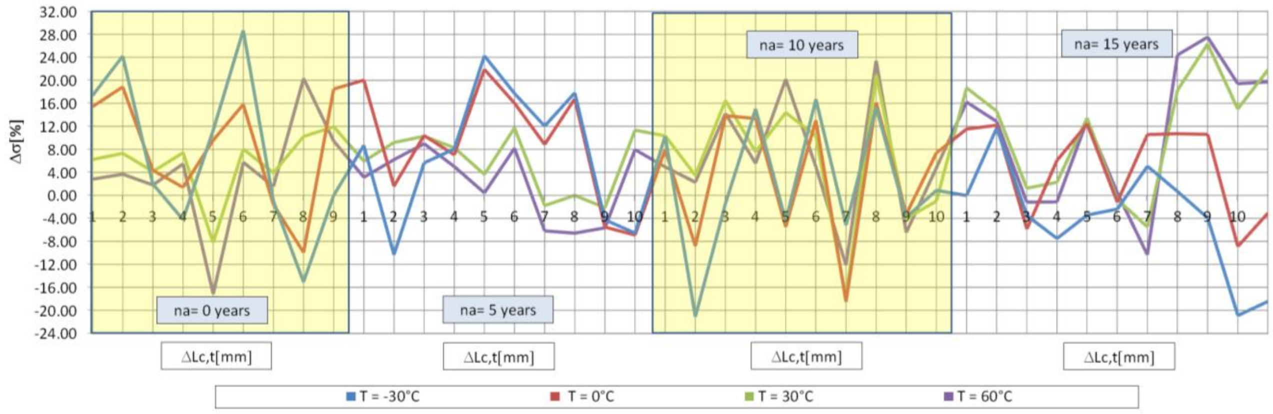

Fig. 15. The graphs of $\Delta\sigma$ (L_c, T) for: T = {-30 ^{0}C, 0 ^{0}C, 30 ^{0}C, 60 ^{0}C} and n_a= {0, 5, 10 and 15 years}

The values of the resultant linear deformation *u* determined by compression and traction for n_a= {0, 5, 10 and 15 years} are shown in table 3.

Table 3: The resultant linear deformations *u* for: T = {-30 ^{0}C, 0 ^{0}C, 30 ^{0}C, 60 ^{0}C} and n_a= {0, 5, 10, 15 years}

n_a [years]	$L_{c,\,t}$ [mm]	T [°C]				T [°C]			
		-30°	0°	-30°	0°	-30°	0°	-30°	0°
		u_c [mm] / the compression loads				u_t [mm] / the traction loads			
0	0	0.869	0.837	0.805	0.777	0.869	0.837	0.805	0.777
	1	0.695	0.704	0.715	0.728	0.652	0.660	0.671	0.685
	2	0.675	0.683	0.693	0.704	0.596	0.603	0.612	0.622
	3	0.673	0.681	0.690	0.700	0.619	0.628	0.638	0.651
	4	0.656	0.664	0.673	0.684	0.622	0.631	0.642	0.656
	5	0.635	0.626	0.619	0.614	0.624	0.628	0.634	0.641
	6	0.623	0.632	0.645	0.659	0.618	0.626	0.637	0.650
	7	0.669	0.676	0.685	0.694	0.618	0.624	0.634	0.646
	8	0.654	0.661	0.670	0.680	0.598	0.604	0.611	0.611
	9	0.636	0.644	0.655	0.666	0.602	0.609	0.617	0.629
	10	0.671	0.678	0.686	0.696	0.614	0.621	0.631	0.642
5	0	0.938	0.904	0.871	0.841	0.938	0.904	0.871	0.841
	1	0.761	0.769	0.780	0.793	0.709	0.715	0.724	0.733
	2	0.728	0.736	0.745	0.757	0.675	0.683	0.693	0.705
	3	0.727	0.735	0.745	0.757	0.672	0.678	0.686	0.695
	4	0.708	0.712	0.720	0.730	0.700	0.711	0.723	0.736
	5	0.697	0.702	0.709	0.718	0.685	0.692	0.700	0.711
	6	0.720	0.719	0.719	0.720	0.675	0.682	0.691	0.703
	7	0.727	0.720	0.713	0.706	0.644	0.636	0.632	0.639
	8	0.718	0.707	0.699	0.696	0.671	0.679	0.689	0.700
	9	0.687	0.695	0.704	0.714	0.698	0.701	0.707	0.713
	10	0.693	0.699	0.707	0.719	0.699	0.703	0.710	0.717
10	0	1.011	0.974	0.944	0.916	1.011	0.974	0.944	0.916
	1	0.836	0.845	0.855	0.866	0.840	0.842	0.845	0.851
	2	0.805	0.815	0.825	0.837	0.711	0.715	0.721	0.729
	3	0.807	0.816	0.826	0.839	0.737	0.748	0.761	0.776
	4	0.805	0.811	0.819	0.828	0.731	0.729	0.735	0.743
	5	0.791	0.796	0.807	0.817	0.754	0.761	0.770	0.780
	6	0.784	0.790	0.797	0.807	0.748	0.744	0.741	0.739
	7	0.788	0.796	0.80	0.814	0.708	0.710	0.714	0.722
	8	0.795	0.793	0.795	0.802	0.755	0.752	0.759	0.769
	9	0.797	0.789	0.783	0.779	0.799	0.788	0.799	0.769
	10	0.804	0.811	0.820	0.831	0.761	0.763	0.766	0.771

15	0	1.106	1.076	1.047	1.020	1.106	1.076	1.047	1.020
	1	0.927	0.933	0.941	0.952	0.872	0.869	0.867	0.800
	2	0.887	0.891	0.887	0.884	0.788	0.791	0.797	0.805
	3	0.905	0.914	0.924	0.935	0.777	0.787	0.799	0.812
	4	0.873	0.882	0.893	0.905	0.834	0.837	0.842	0.849
	5	0.843	0.835	0.829	0.831	0.829	0.835	0.843	0.851
	6	0.882	0.873	0.872	0.877	0.808	0.813	0.820	0.830
	7	0.932	0.938	0.948	0.960	0.792	0.783	0.774	0.768
	8	0.871	0.879	0.888	0.898	0.805	0.804	0.806	0.812
	9	0.833	0.839	0.847	0.855	0.812	0.805	0.802	0.800
	10	0.899	0.904	0.910	0.917	0.842	0.836	0.830	0.824

The graphs of curves (in 2-D) corresponding to the resultant linear deformation u = (L_c, T) for n_a = {0, 5, 10 and 15 years}; are graphically shown in fig. 16, while the corresponding graphs (in 3-D) are shown figs. 17-21.

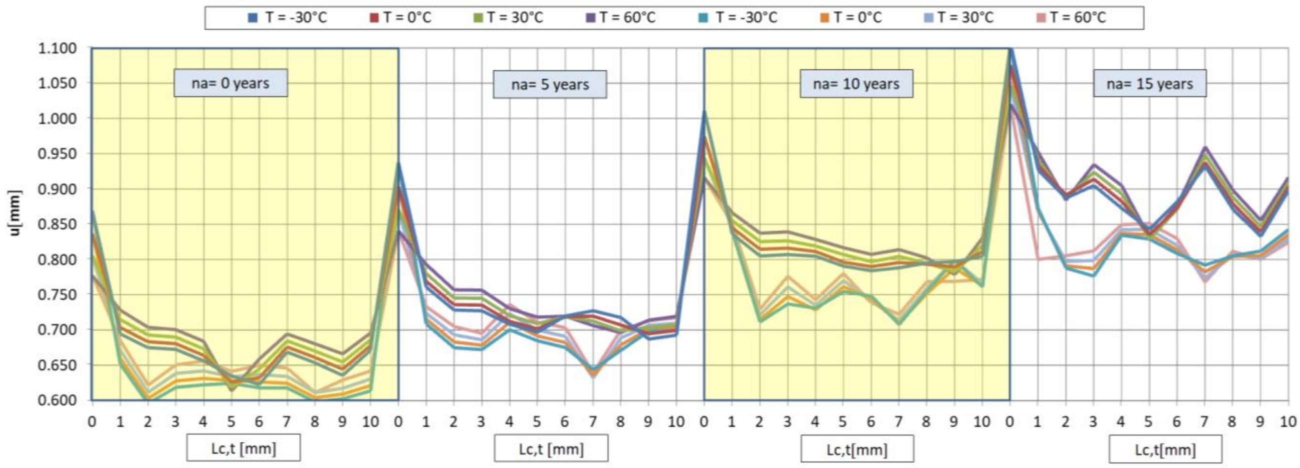

Fig. 16. The graphs of u = ($L_{c,t}$, T) for: T = {-30 ^{0}C, 0 ^{0}C, 30 ^{0}C, 60 ^{0}C} and n_a= {0, 5, 10 and 15 years}

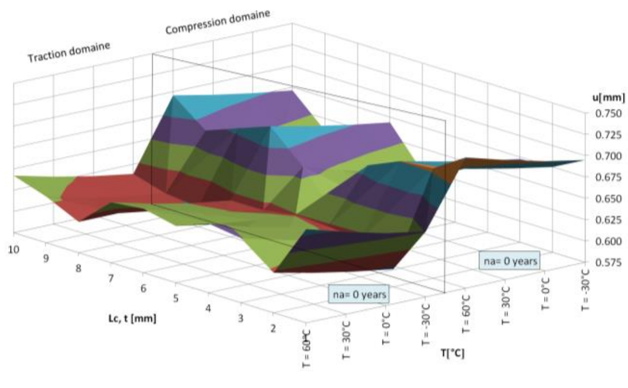

Fig. 17. The graphs of u = (L_c, T) for n_a = 0 years left (traction domain); right (compression domain)

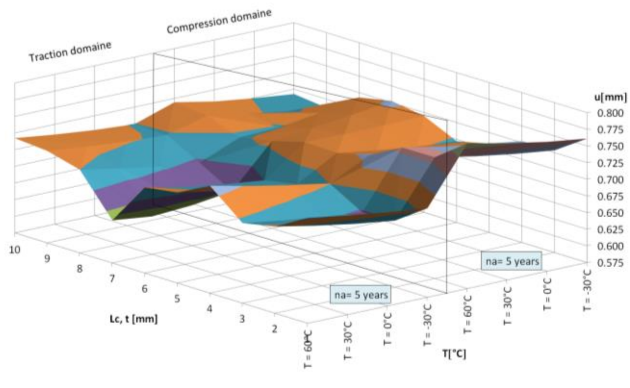

Fig. 18. The graphs of u = (L_c, T) for n_a = 5 years left (traction area); right (compression area)

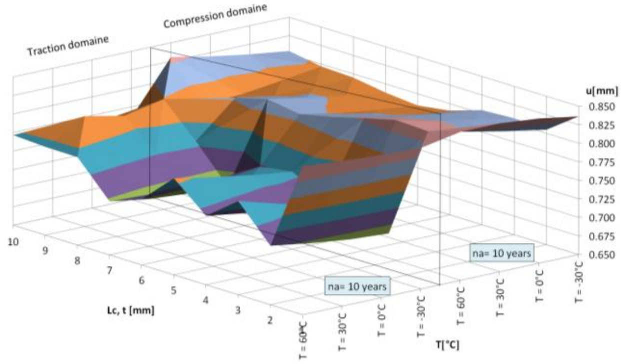

Fig. 19. The graphs of u = (L_c, T) for n_a = 10 years left (traction domain); right (compression domain)

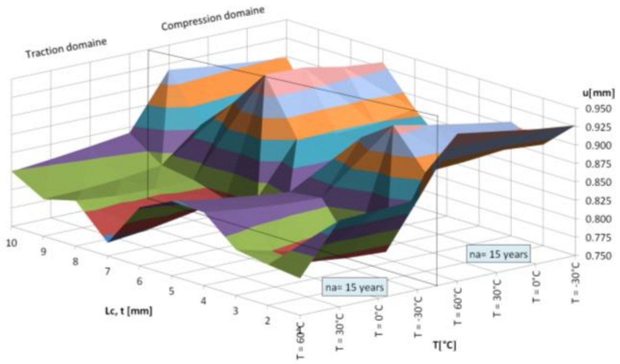

Fig. 20. The graphs of u = (L_c, T) for n_a = 15 years left (traction area); right (compression area)

The graphs of curves u = (L_c, T) with these highlighted details are shown in figs. 21-24.

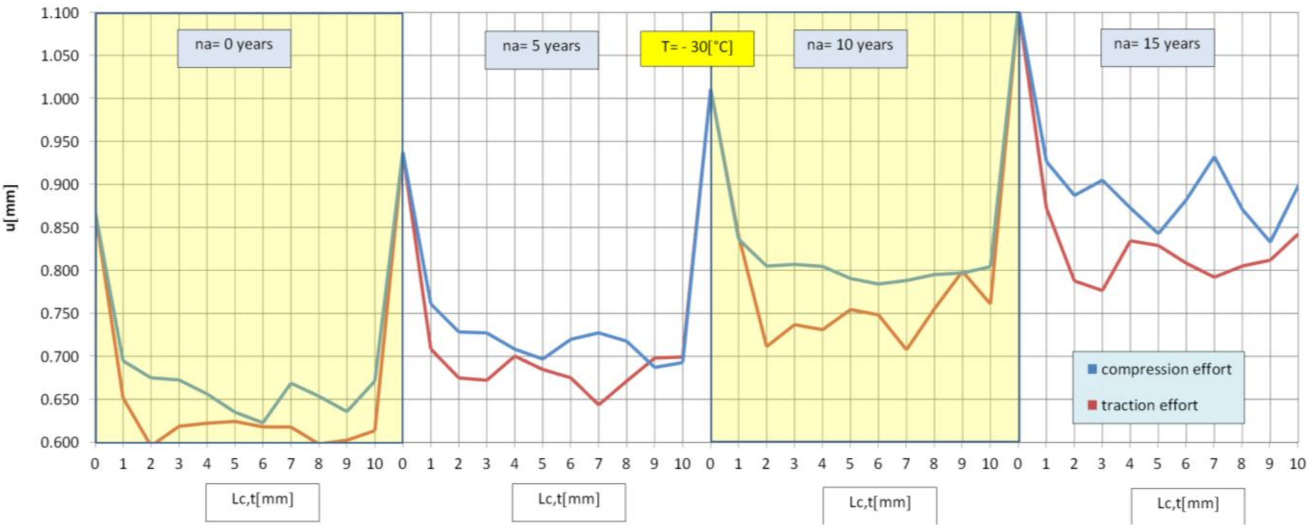

Fig. 21. The graphs of the resulting linear deformations u = f(L_c, T) with highlighted details: (T = -30 ^{0}C; n_a= {0, 5, 10 and 15 years}; blue curve – the compression effort; red curve – the traction effort;

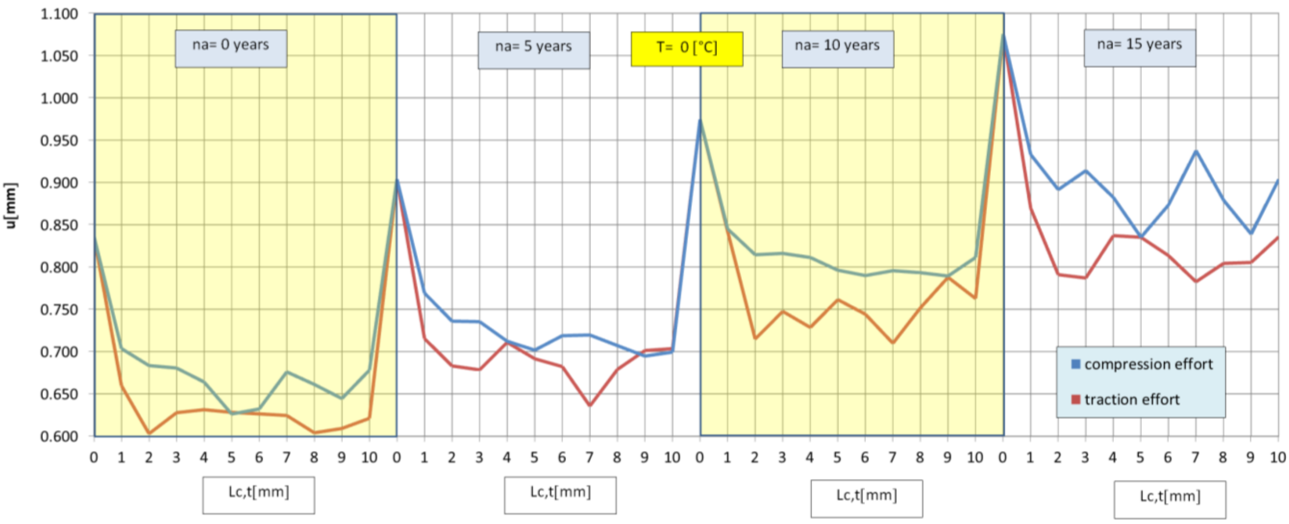

Fig. 22. The graphs of the resulting linear deformations u = f(L_c, T) with highlighted details: (T = 0 ^{0}C; n_a= {0, 5, 10 and 15 years}; blue curve – the compression effort; red curve – the traction effort;

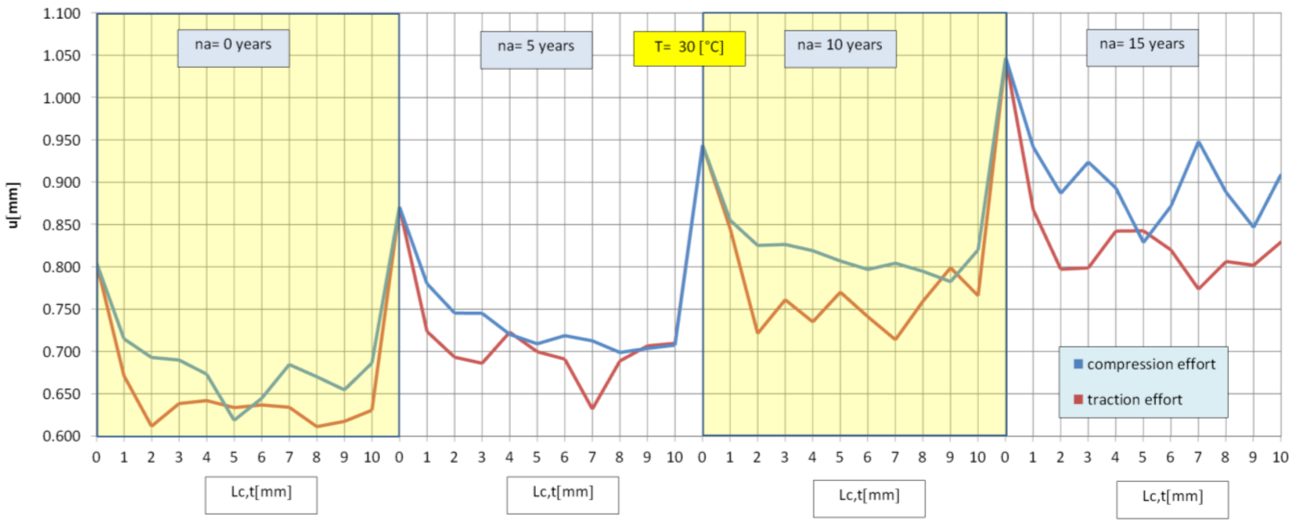

Fig. 23. The graphs of the resulting linear deformations u = f(L_c, T) with highlighted details:
(T = 30 ^{0}C; n_a= {0, 5, 10 and 15 years}; blue curve – the compression effort; red curve – the traction effort;

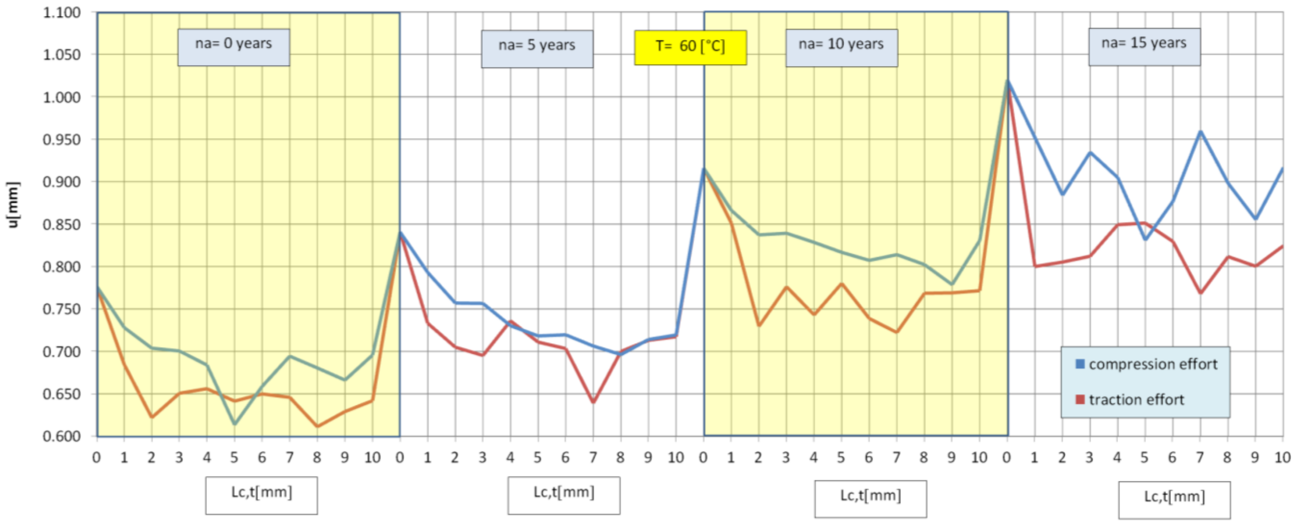

Fig. 24. The graphs of the resulting linear deformations u = f(L_c, T) with highlighted details:
(T = 60 ^{0}C; n_a= {0, 5, 10 and 15 years}; blue curve – the compression effort; red curve – the traction effort;

It was calculated the percentage variation of the resultant linear deformation Δu (L_c, T) given by compression versus the resulting stress state given by traction, using the following formula:

$$\Delta u = \frac{(u_c - u_t)}{u_t} \cdot 100 \; [\%] \tag{1}$$

The percentage variation of Von Mises resultant effort Δu was computed in table 4 and the corresponding graphs (in 2-D) are shown in fig. 25.

Table 4: The percentage variation of resultant liniar deformation Δu for:
T = {-30 ^{0}C, 0 ^{0}C, 30 ^{0}C, 60 ^{0}C} and n_a= {0, 5, 10 and 15 years}

$L_{c,t}$ [mm]	T [°C]				T [°C]			
	-30°	0°	-30°	0°	-30°	0°	-30°	0°
	Δu [mm]				Δu [mm]			
	n_a = 0 [years]				n_a = 5 [years]			
1	6.62	6.65	6.51	6.35	7.41	7.52	7.81	8.16
2	13.31	13.36	13.29	13.17	7.92	7.75	7.52	7.38

3	8.72	8.42	8.06	7.66	8.19	8.40	8.60	8.82
4	5.48	5.18	4.87	4.26	1.14	0.18	-0.35	-0.78
5	1.73	-0.31	-2.37	-4.34	1.78	1.47	1.34	1.02
6	0.76	0.93	1.23	1.37	6.62	5.36	4.01	2.30
7	8.26	8.26	7.96	7.52	13.01	13.22	12.77	10.53
8	9.30	9.47	9.65	11.34	6.90	4.16	1.46	-0.52
9	5.53	5.81	6.04	5.90	-1.56	-0.93	-0.42	0.13
10	9.40	9.17	8.83	8.38	-0.94	-0.58	-0.30	0.29
	n_a = 10 [years]				n_a = 15 [years]			
1	-0.44	0.35	1.16	1.78	6.22	7.31	8.53	18.99
2	13.17	13.96	14.43	14.78	12.63	12.71	11.24	9.79
3	9.51	9.17	8.58	8.11	16.53	16.12	15.66	15.09
4	10.08	11.35	11.44	11.50	4.58	5.40	6.03	6.54
5	4.79	4.57	4.78	4.69	1.66	0.00	-1.64	-2.37
6	4.80	6.14	7.55	9.28	9.15	7.36	6.32	5.70
7	11.39	12.10	12.66	12.70	17.71	19.82	22.57	24.99
8	5.25	5.51	4.65	4.39	8.18	9.29	10.14	10.65
9	-0.24	0.19	-2.05	1.26	2.58	4.18	5.58	6.88
10	5.71	6.37	7.06	7.67	6.66	8.14	9.65	11.18

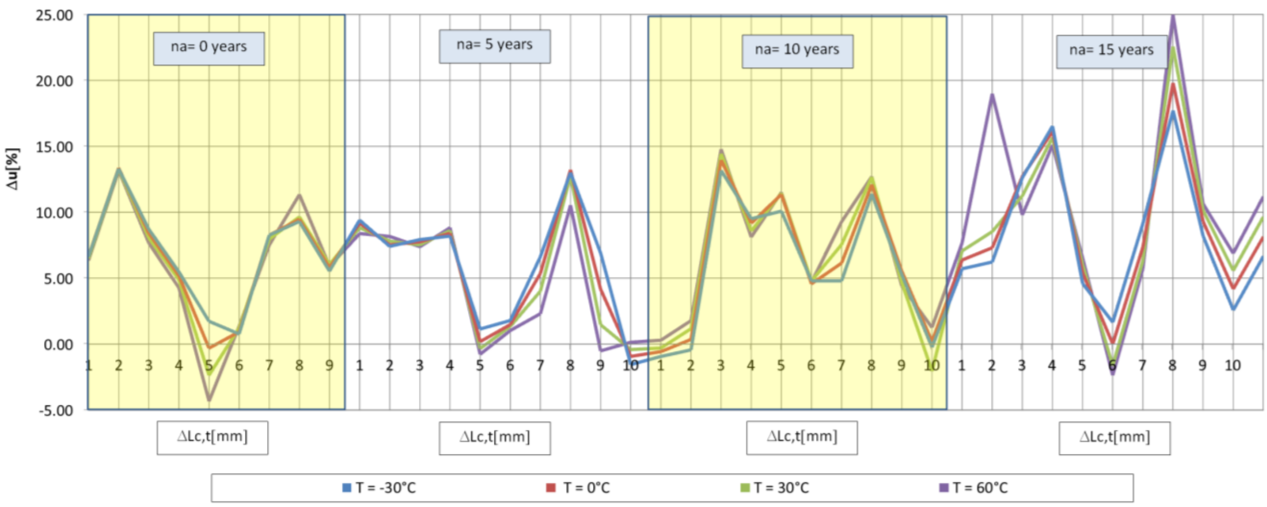

Fig. 25. The graphs of Δu (L_c, T) for: T = {-30 ^{0}C, 0 ^{0}C, 30 ^{0}C, 60 ^{0}C} and n_a= {0, 5, 10 and 15 years}

3. Conclusions

Following the numerical analyses and the resulting graphs it has been found that:
- the state of deformations are amplified with the increase of compression and traction loads;
- the state of efforts are amplified with the increase of compression and traction loads, and by the decreasing of the working temperature;
- for the compression loads, n_a= 15 years, T = -30 ^{0}C, σ_{max} = 760.64 MPa > σ_a = 710 MPa, and L_c = 2 mm;
- the percentage variation of Von Mises resultant effort (Δσ) for the compression loads is greater with Δσ = 28.68% than the traction loads;
- the values of the resultant linear deformation *u* for compression loads are greater than traction loads. Also, the resultant linear deformation *u* is amplified with the increase of the working period;
- the resultant linear deformation (u) for the compression loads is greater than the traction loads and is amplified with the increase of the working period;
- the percentage variation of resultant linear deformation (Δu) is greater with Δu = 25 [%] for the compression loads is greater than the traction loads;
- it can be appreciated that the most disadvantageous state of stresses appears in case the compression loads.

References

[1] Ghiţă, C. Mirela, Anton C. Micu, Mihai Ţălu and Ştefan Ţălu. “Shape optimization of a thoroidal methane gas tank for automotive industry.” *Annals of Faculty of Engineering Hunedoara - International Journal of Engineering, Hunedoara, Romania*, Tome X, Fascicule 3 (2012): 295-297.
[2] Ghiţă, C. Mirela, Anton C. Micu, Mihai Ţălu and Ştefan Ţălu. “Shape optimization of vehicle's methane gas tank.“ *Annals of Faculty of Engineering Hunedoara - International Journal of Engineering, Hunedoara, Romania*, Tome X, Fascicule 3 (2012): 259-266.
[3] Ghiţă, C. Mirela, Anton C. Micu, Mihai Ţălu, Ştefan Ţălu and Ema I. Adam. “Computer-Aided Design of a classical cylinder gas tank for the automotive industry.“ *Annals of Faculty of Engineering Hunedoara - International Journal of Engineering, Hunedoara*, *Romania*, Tome XI, Fascicule 4 (2013): 59-64.
[4] Ghiţă, C. Mirela, Anton C. Micu, Mihai Ţălu and Ştefan Ţălu. “3D modelling of a shrink fitted concave ended cylindrical tank for automotive industry.“ *Acta Technica Corviniensis – Bulletin of Engineering, Hunedoara, Romania*, Tome VI, Fascicule 4 (2013): 87-92.
[5] Ghiţă, C. Mirela, Anton C. Micu, Mihai Ţălu and Ştefan Ţălu. “3D modelling of a gas tank with reversed end up covers for automotive industry.“ *Annals of Faculty of Engineering Hunedoara - International Journal of Engineering, Hunedoara*, *Romania*, Tome XI, Fascicule 3 (2013): 195-200.
[6] Ghiţă, C. Mirela, Ştefan C. Ghiță, Ştefan Ţălu and Simona Rotaru. “Optimal design of cylindrical rings used for the shrinkage of vehicle tanks for compressed natural gas.“ *Annals of Faculty of Engineering Hunedoara - International Journal of Engineering, Hunedoara*, Tome XII, Fascicule 3 (2014): 243-250.
[7] Vintilă, Daniela, Mihai Ţălu and Ştefan Ţălu. “The CAD analyses of a torospheric head cover of a pressurized cylindrical fuel tank after the crash test.” *Magazine of Hydraulics, Pneumatics, Tribology, Ecology, Sensorics, Mechatronics (HIDRAULICA)*, no. 4 (December 2017): 57-66.
[8] Bică, Marin, Mihai Ţălu and Ştefan Ţălu. “Optimal shapes of the cylindrical pressurized fuel tanks.” *Magazine of Hydraulics, Pneumatics, Tribology, Ecology, Sensorics, Mechatronics (HIDRAULICA)*, no. 4 (December 2017): 6-17.
[9] Ţălu, Mihai. "The influence of the corrosion and temperature on the Von Mises stress in the lateral cover of a pressurized fuel tank." *Magazine of Hydraulics, Pneumatics, Tribology, Ecology, Sensorics, Mechatronics (HIDRAULICA)*, no. 4 (December 2017): 89-97.
[10] Ţălu, Ştefan and Mihai Ţălu. "The influence of deviation from circularity on the stress of a pressurized fuel cylindrical tank." *Magazine of Hydraulics, Pneumatics, Tribology, Ecology, Sensorics, Mechatronics (HIDRAULICA)*, no. 4 (December 2017): 34-45.
[11] Ţălu, Mihai and Ştefan Ţălu. "Design and optimization of pressurized toroidal LPG fuel tanks with variable section." *Magazine of Hydraulics, Pneumatics, Tribology, Ecology, Sensorics, Mechatronics (HIDRAULICA)*, no. 1 (March 2018): 32-41.
[12] Ţălu, Mihai and Ştefan Ţălu. "Analysis of temperature resistance of pressurized cylindrical fuel tanks." *Magazine of Hydraulics, Pneumatics, Tribology, Ecology, Sensorics, Mechatronics (HIDRAULICA)*, no. 1 (March 2018): 6-15.
[13] Ţălu, Ştefan and Mihai Ţălu. "Algorithm for optimal design of pressurized toroidal LPG fuel tanks with constant section described by imposed algebraic plane curves." *Magazine of Hydraulics, Pneumatics, Tribology, Ecology, Sensorics, Mechatronics (HIDRAULICA)*, no. 2 (June 2018): 14-21.
[14] Ţălu, Mihai and Ştefan Ţălu. "The optimal CAD design of a 3D hexagonal toroid with regular hexagonal cross-section used in manufacturing of LPG storage tanks." *Magazine of Hydraulics, Pneumatics, Tribology, Ecology, Sensorics, Mechatronics (HIDRAULICA)*, no. 2 (June 2018): 49-56.
[15] Ţălu, Mihai and Ştefan Ţălu. "The influence of corrosion and temperature variation on a CNG storage tank with a combined form consisting of a torus and a sphere." *Magazine of Hydraulics, Pneumatics, Tribology, Ecology, Sensorics, Mechatronics (HIDRAULICA)*, no. 4 (December 2019): 93-104.
[16] Ţălu, Mihai and Ştefan Ţălu. "Optimal design of a CNG storage tank with a combined form consisting of a torus and a sphere." *Magazine of Hydraulics, Pneumatics, Tribology, Ecology, Sensorics, Mechatronics (HIDRAULICA)*, no. 4 (December 2019): 73-82.
[17] Ţălu, Mihai and Ştefan Ţălu. “The influence of corrosion and temperature variation on the minimum safety factor of a 3D hexagonal toroid with regular hexagonal cross-section used in manufacturing of LPG storage tanks.“ *Magazine of Hydraulics, Pneumatics, Tribology, Ecology, Sensorics, Mechatronics (HIDRAULICA)*, no. 3 (September 2018): 16-25.
[18] Ţălu, Ştefan and Mihai Ţălu. "The influence of corrosion and pressure variation on the minimum safety factor of a 3D hexagonal toroid with regular hexagonal cross-section used in manufacturing of LPG storage tanks." *Magazine of Hydraulics, Pneumatics, Tribology, Ecology, Sensorics, Mechatronics (HIDRAULICA)*, no. 3 (September 2018): 39-45.
[19] Ţălu, Mihai and Ştefan Ţălu. "Study of temperature–corrosion–torsion affecting factors on the shape of a toroidal LPG tank using the finite element method." *Magazine of Hydraulics, Pneumatics, Tribology, Ecology, Sensorics, Mechatronics (HIDRAULICA)*, no. 1 (March 2020): 21-32.

[20] Ţălu, Ştefan and Mihai Ţălu. "Numerical analysis of the influence of uniaxial compression loads on the shape of a toroidal LPG tank." *Magazine of Hydraulics, Pneumatics, Tribology, Ecology, Sensorics, Mechatronics (HIDRAULICA)*, no. 1 (March 2020): 47-58.
[21] Ţălu, Mihai and Ştefan Ţălu. "Stress and deformation analysis under bending and torsional loads of a toroidal LPG tank based on the finite element analysis." *Magazine of Hydraulics, Pneumatics, Tribology, Ecology, Sensorics, Mechatronics (HIDRAULICA)*, no. 1 (March 2020): 88-101.
[22] Oprițoiu, Petre. "Analysis of uniaxial traction loads on the 3-D geometry of a toroidal LPG storage tank." *Magazine of Hydraulics, Pneumatics, Tribology, Ecology, Sensorics, Mechatronics (HIDRAULICA)*, no. 2 (June 2020): 15-26.
[23] Ţălu, Ştefan and Mihai Ţălu. "Constructive CAD variants of toroidal LPG fuel tanks used in automotive Industry." *Advances in Intelligent Systems Research* 159 (2018): 27-30. DOI: 10.2991/mmsa-18.2018.7.
[24] Ţălu, Mihai and Ştefan Ţălu. "3D geometrical solutions for toroidal LPG fuel tanks used in automotive industry." *Advances in Intelligent Systems Research* 151 (2018): 189-193. DOI: 10.2991/cmsa-18.2018.44.
[25] Ţălu, Mihai and Ştefan Ţălu. "Optimal engineering design of a pressurized paralepipedic fuel tank." *Annals of Faculty of Engineering Hunedoara - International Journal of Engineering, Hunedoara, Romania*, Tome XVI, Fascicule 2 (2018): 193-200.
[26] Ţălu, Ştefan and Mihai Ţălu. "The Influence of corrosion on the vibration modes of a pressurized fuel tank used in automotive industry." *DEStech Transactions on Materials Science and Engineering,* (2018): 1-6. DOI: 10.12783/dtmse/icmsa2018/20560.
[27] Oprițoiu, Petre. PhD thesis: *Cercetări privind transferul termic și al pierderilor de presiune la un schimbător de căldură din metal poros / Research on heat transfer and pressure losses through porous metal heat exchanger.* Technical University of Cluj-Napoca, Romania, Faculty of Mechanics, 2014.
[28] Oprițoiu, Petre. "Fluid flow and pressure drop simulation in aluminium foam heat exchanger." *Acta Tech. Napocensis: Civil Eng. & Arch*., no. 50 (2007): 101-112.
[29] Oprițoiu, Petre. "Heat transfer performance analysis in porous heat exchanger." *Magazine of Hydraulics, Pneumatics, Tribology, Ecology, Sensorics, Mechatronics (HIDRAULICA)*, no. 3 (September 2015): 32-41.
[30] Oprițoiu, Petre. "Rans simulation of combined flow and heat transfer through open-cell aluminum foam heat sink." *Magazine of Hydraulics, Pneumatics, Tribology, Ecology, Sensorics, Mechatronics (HIDRAULICA)*, no. 3 (September 2013): 15-25.
[31] Oprițoiu, Petre. "Prediction of turbulent flow using upwind discretization scheme and k-ε turbulence model for porous heat exchanger." *Magazine of Hydraulics, Pneumatics, Tribology, Ecology, Sensorics, Mechatronics (HIDRAULICA)*, no. 2 (June 2016): 88-97.
[32] Oprițoiu, Petre. "Validation of porous heat exchanger simulation model." Paper presented at International Conference and Exhibition of Hydraulics & Pneumatics HERVEX 2014, Călimăneşti-Căciulata, Romania, 5-7 noiembrie 2014.
[33] Ţălu, Ştefan and Mihai Ţălu. "CAD generating of 3D supershapes in different coordinate systems. "*Annals of Faculty of Engineering Hunedoara - International Journal of Engineering, Hunedoara, Romania*, Tome VIII, Fascicule 3 (2010): 215-219.
[34] Ţălu, Ştefan and Mihai Ţălu. "A CAD study on generating of 2D supershapes in different coordinate systems. "*Annals of Faculty of Engineering Hunedoara - International Journal of Engineering, Hunedoara, Romania*, Tome VIII, Fascicule 3 (2010): 201-203.
[35] Domanski, Jerzy and Zywica Grzegorz. "Optimization of the construction of a pressure tank using CAD/CAE systems." *Technical Sciences* 10 (2007): 41-59. DOI: 10.2478/v10022-007-0006-4.
[36] Nedelcu, Dorian. *Digital Prototyping and Numerical Simulation with SolidWorks / Proiectare și simulare numerică cu SolidWorks*. Timişoara, Eurostampa Publishing House, 2011.
[37] Ţălu, Mihai. *Mecanica fluidelor. Fluid mechanics. The monodimensional laminar flow / Curgeri laminare monodimensionale.* Craiova, Universitaria Publishing House, 2016.
[38] Țălu, Mihai. *Hydraulic pressure loss in technical piping with annular section. Numerical calculation and C.F.D. / Pierderi de presiune hidraulică în conducte tehnice cu secțiune inelară. Calcul numeric și analiză C.F.D.* Craiova, Universitaria Publishing House, 2016.
[39] Niţulescu, Theodor and Ştefan Ţălu. *Applications of descriptive geometry and computer aided design in engineering graphics / Aplicaţii ale geometriei descriptive şi graficii asistate de calculator în desenul industrial.* Cluj-Napoca, Risoprint Publishing House, 2001.
[40] Bîrleanu, Corina and Ştefan Ţălu. *Organe de maşini. Machine elements. Designing and computer assisted graphical representations / Proiectare şi reprezentare grafică asistată de calculator.* Cluj-Napoca, Victor Melenti Publishing House, 2001.
[41] Ţălu, Ştefan. *AutoCAD 2017*. Cluj-Napoca, Napoca Star Publishing House, 2017.
[42] Racocea, Cristina and Ştefan Ţălu. *The axonometric representation of technical geometric shapes / Reprezentarea formelor geometrice tehnice în axonometrie.* Cluj-Napoca, Napoca Star Publishing House, 2011.